Radial-basis-function level-set-based regularized Gauss–Newton-filter reconstruction scheme for dynamic shape tomography

Naren Naik,[1,*] Rick Beatson,[2,4] and Jerry Eriksson[3,5]

[1]Department of Electrical Engineering and Center for Lasers and Photonics, Indian Institute of Technology, Kanpur, Kanpur 208016, India

[2]Department of Mathematics and Statistics, University of Canterbury, Private Bag 4800, Christchurch 8140, New Zealand

[3]Department of Computing Science, Umeå University, S-901, 87 Umeå, Sweden

[4]e-mail: rick.beatson@canterbury.ac.nz

[5]e-mail: jerry@cs.umu.se

*Corresponding author: nnaik@iitk.ac.in

Received 9 June 2014; revised 18 August 2014; accepted 31 August 2014; posted 3 September 2014 (Doc. ID 213674); published 9 October 2014

The dynamic reconstruction problem in tomographic imaging is encountered in several applications, such as species determination, the study of blood flow through arteries/veins, motion compensation in medical imaging, and process tomography. The reconstruction method of choice is the Kalman filter and its variants, which, however, are faced by issues of filter tuning. In addition, since the time-propagation models of physical parameters are typically very complex, most of the time, a random walk model is considered. For geometric deformations, affine models are typically used. In our work, with the objectives of minimizing tuning issues and reconstructing time-varying geometrically deforming features of interest with affine in addition to pointwise-normal scaling motions, a novel level-set-based reconstruction scheme for ray tomography is proposed for shape and electromagnetic parameters using a regularized Gauss–Newton-filter-based scheme. We use an implicit Hermite-interpolation-based radial basis function representation of the zero level set corresponding to the boundary curve. Another important contribution of the paper is an evaluation of the shape-related Frechet derivatives that does not need to evaluate the pointwise Jacobian (the ray-path matrix in our ray-tomography problem). Numerical results validating the formulation are presented for a straight ray-based tomographic reconstruction. To the best of our knowledge, this paper presents the first tomographic reconstruction results in these settings.

OCIS codes: (110.3010) Image reconstruction techniques; (110.6955) Tomographic imaging; (110.6960) Tomography.

http://dx.doi.org/10.1364/AO.53.006872

1. Introduction

The problem of reconstruction of time-varying parameters from tomographic measurements appears in several situations, such as process tomography [1], biomedical tomography [2–4], and species analysis [5,6]. Typical solution schemes in the literature for such problems have been via the use of Kalman filters and their variants, such as the nonlinear extended Kalman filter in applications such as electrical impedance tomography [1], diffuse optical

1559-128X/14/296872-13$15.00/0

tomography [2,3], infrared species tomography of transient flow fields [5], and reconstruction of a time-varying state vector containing physical and/or shape parameters, or via the use of variational schemes such as in [7,8].

The main issues in such reconstructions are typically about having an awareness of the nature of dynamics of the state, tuning the Kalman filter for the various filter covariances, and knowing the amount of information that can be realistically reconstructed from the typically limited data available in situations in which the object undergoes a transition between two measurements.

If the state is a pointwise physical parameter (such as refractive index, absorption coefficient, or electrical impedance as the case may be), its dynamics are typically not easily known and it is mostly modeled as a random walk. Considering the limited data available in situations in subsurface imaging or high-speed imaging, the object is typically represented in terms of its shape and any physical/electromagnetic parameter characterizing it. In such representations, the dynamics have been typically assumed to be of the class of affine transformations [7] with possibly unknown components [8]. Also, considering that the actual pointwise state dynamics can be very complex, estimating the dynamics in a geometrical deformation setting gives extremely valuable insight into the actual behavior of such time variations.

"Shape-based" approximate reconstruction schemes broadly fall into two categories. The first class has as unknowns the coefficients in an explicit parametric representation for the boundary curve(s), while in the latter class, the unknowns are the values of a set function representing the image, with the zero level set of that function implicitly representing the boundary. While the first (explicit-representation) class of schemes (as in [9–14]) has the advantage of fewer unknowns, which is useful in potential three-dimensional reconstructions, the second (implicit-representation) class [6,15,16] is better suited to handle topological changes in the evolving shape of the boundary. Radial basis function (RBF)-based implicit-representation reconstruction schemes were first suggested in [17] followed by recent works such as [18,19], extending the capability of the approaches in [10,14] by allowing for topological changes, while retaining their advantage over conventional implicit-representation schemes of having few unknowns. A detailed literature survey of these various classes of schemes is given in [10,13,14,17,18].

In recent works [18,19], a compactly supported RBF-based parameterized level-set representation with centers in the interior of the domain (the centers in [17] are placed on the boundary) is used to solve single and multi-objective reconstruction problems in static nonlinear tomographic settings.

The contribution of our present work is to set up the framework for the time-varying shape-reconstruction problem with unknown boundary dynamics in an RBF-based level-set parametrization with respect to a regularized Gauss–Newton-filter scheme. In addition, we assume the class of shape transitions to be of a nonlinear kind, consisting of the affine class [20] in addition to a pointwise-normal scaling. Another contribution of the paper is an evaluation of the shape-related Frechet derivatives that does not need to evaluate the pointwise Jacobian (the ray-path matrix in our ray-tomography problem).

The Gauss–Newton filter [21] is a batch estimator of time-varying states and overcomes to quite an extent the tuning issues of nonlinear Kalman filtering. Also, scaling along the normal at a boundary point is a deformation that is natural with respect to level-set schemes since only boundary perturbations along the normal are considered in these. This "naturalness" of normal deformations is emphasized in the case of Hermite-RBF-interpolation-based representations with centers on the boundary, since the normals at the RBF centers are reconstructed along with the center coordinates. To the best of our knowledge, this paper presents the first tomographic reconstruction results in these settings.

An object's boundary is defined implicitly as the zero level set of an RBF fitted to boundary parameters comprising the locations of a few points on the curve (namely the RBF centers) and the normal vectors at those points. The e.m. parameter reconstructed is the difference of the refractive indices of the object and the ambient space, and is represented by coefficients in a suitable global basis. An objective functional w.r.t. time-varying boundary and e.m. parameters is set up, and required Frechet derivatives are calculated. Reconstructions are obtained by using an iteratively regularized Gauss–Newton-filtering scheme for this almost rank-deficient problem.

The layout of this paper is as follows. Section 2 gives the problem formulation, and Section 3 evaluates the shape derivatives for the regularized Gauss–Newton solution scheme. Validating numerical studies in straight-path tomography test cases are carried out in Section 4. Section 5 presents the conclusions of our study. Appendix A gives the RBF interpolation matrix and level-set derivative, and Appendix B gives the Jacobian matrix corresponding to the state-transition model considered in our work.

2. Problem Statement

The fundamental reconstruction problem is the recovery of a time-varying spatially finitely supported electromagnetic parameter such as the refractive index or attenuation coefficient $\alpha(\mathbf{r},t)$ from line-integral measurements at different views corresponding to different time instants.

The line-integral measurements obtained at each time instant can be written as

$$p_L(t) = \int_L \alpha(\mathbf{r},t)\mathrm{d}s, \tag{1}$$

where L corresponds to the line in object space along which the ray integral is taken, $\alpha(\mathbf{r},t)$ being the spatially and time-varying refractive-index/attenuation distribution under interrogation.

Observing that $\alpha(\mathbf{r},t)$ contains information about the parameter values as well as the shape, considering, without loss of generality, homogeneous inclusions in the background, we can express the parameter at a point in the image space as

$$\alpha(\mathbf{r},t) = \alpha^g(\mathbf{r}) H_\rho[s(\mathbf{r};t)], \tag{2}$$

where $s(.;t)$ is a level-set-based representation of the image (see [22] and references therein) at a time instant t, with $\{\mathbf{r}{:}s(\mathbf{r};t)=0\}$ representing the boundary $\partial\Omega$ at time instant t of the object(s) under consideration supported in region Ω; $H_\rho[.]$ is a Heaviside function taken in a suitable limiting sense [23]; and the field quantity $\alpha^g(.)$ can be considered as a "ghost" parameter value manifesting itself through $H(.)$. Without loss of conceptual generality we consider $\alpha^g(\mathbf{r}) = \alpha_0$, with α_0 being a constant independent of position.

The approximation to the Heaviside mentioned above is

$$H_\rho(t) := \begin{cases} 0 & \text{if } t < -\rho \\ \frac{1}{2}\left\{1 + \frac{t}{\rho} + \frac{1}{\pi}\sin\left(\frac{\pi t}{\rho}\right)\right\} & \text{if } t \in [-\rho,\rho]. \\ 1 & \text{if } t > \rho \end{cases} \tag{3}$$

There are many ways in which one can represent the boundary curve/surface $s(\mathbf{r}) = 0$ (suppressing the time dependence for ease of notation). In an explicit parametrization, this boundary has been described in terms of a spline basis [9,12,14] in two dimensions or with spherical harmonics [10] in three dimensions. In implicit formulations [6,17–19], typically the shape unknowns are the values of the function $s(\mathbf{r})$ on the reconstruction grid. In [17] with the objective of retaining an implicit representation coupled with significant search-space-dimensionality reduction (as in explicit schemes), we represent $s(\mathbf{r})$ as a RBF via a Hermite interpolation scheme to fit a few on-curve points (called centers of the RBF, and denoted by $\mathbf{r}_1^c \ldots \mathbf{r}_m^c$) and the normal unit vectors at those points (denoted by $\mathbf{n}_1 \ldots \mathbf{n}_m$, where $\mathbf{n}_i \equiv (\cos\theta_i^c, \sin\theta_i^c)$ for some θ_i^c).

Our Hermite interpolation problem can be stated as follows [17]:

Given values $b_1, \ldots, b_{2\,m}$ find a continuously differentiable function $s{:}IR^d \to IR$ such that

$$\mu_i(s) \equiv s(\mathbf{r}_i^c) = b_i \quad \text{and} \quad \mu_{i+m}(s) \equiv \mathbf{n}_i \cdot (\nabla s)(\mathbf{r}_i^c) = b_{m+i}, \quad \text{for } 1 \le i \le m. \tag{4}$$

These $2m$ functionals are linearly independent provided the points $\mathbf{r}_i^c$, $1 \le i \le m$, are distinct. Let π_{k-1}^d denote the space of polynomials of degree at most $k-1$ in d variables. Having chosen a twice continuously differentiable basic function Φ, conditionally positive definite of order k in the appropriate sense, we can write the level-set solutions to the RBF Hermite interpolation problem as an RBF of the form

$$s(\mathbf{r}) = p(\mathbf{r}) + \sum_{j=1}^{m} [c_j \Phi(\mathbf{r} - \mathbf{r}_j^c) - d_j (D_{n_j}\Phi)(\mathbf{r} - \mathbf{r}_j^c)], \tag{5}$$

where $p(.)$ is a polynomial (typically of low order), $\Phi(.) \equiv \phi(\|.\|)$, with ϕ being a (usually unbounded and noncompactly supported) real-valued function on $[0,\infty]$ called the basic function, and $D_{n_j}\psi(t) \equiv \mathbf{n}_j \cdot (\nabla\psi)(t)$ denoting the directional derivative functional w.r.t a unit normal $\mathbf{n}_j$. The coefficients c and d are the RBF coefficients.

Applying the interpolation conditions we obtain the RBF Hermite interpolation problem in matrix form:

$$\begin{bmatrix} A & P \\ P^T & O \end{bmatrix} \begin{bmatrix} \boldsymbol{\lambda} \\ \mathbf{a} \end{bmatrix} = \begin{bmatrix} \mathbf{b} \\ 0 \end{bmatrix}, \tag{6}$$

with the entries $A_{ij} = \mu_i^{\mathbf{r}} \mu_j^{\mathbf{t}} \Phi(\mathbf{r}-\mathbf{t})$, $P_{ij} = \mu_i(p_j)$, where $p(\mathbf{r}) = \sum_{l=1}^{L} a_l p_l(\mathbf{r})$ for some basis $\{p_1, \ldots, p_\ell\}$ for the space π_{k-1}^d, and, $\boldsymbol{\lambda} \equiv \binom{\mathbf{c}}{\mathbf{d}}$. The expressions for the entries in the matrices A and P of Eq. (A1) are given in [17] and summarized in Appendix A for completeness.

We are reconstructing a signed distance function, which is zero on the curve and has a unit directional derivative in the direction of the inward normal. Thus, the right-hand side values we will use are $b_i = 0$ for $1 \le i \le m$, and $b_i = 1$ for $m+1 \le i \le 2m$. Hence, given the RBF centers $\{\mathbf{r}_j^c\}$, and the unit normal vectors at those points $\{\mathbf{n}_j = (\cos(\theta_j^c), \sin(\theta_j^c))\}$, we obtain the coefficient vectors $\mathbf{a}$ and $\boldsymbol{\lambda}$ for our RBF approximation (5) by forming and solving the linear system (A1).

In this work, we use the Hermite-interpolation-based representation of [17]. In the two-dimensional setting considered in our work, $\mathbf{r} \equiv (x,y)$, and we have as shape parameters the RBF-center coordinates $\{x_q^c | q = 1 \ldots M_p\}$, $\{y_q^c | q = 1 \ldots M_p\}$ along with the unit normals represented by the respective angles $\{\theta_q^c | q = 1 \ldots M_p\}$, corresponding in vector notation to $\mathbf{x^c}$, $\mathbf{y^c}$, and $\boldsymbol{\theta^c}$, respectively. Further, for each time instant, we augment these variables with the geometric-transformation variables needed, such as those related to translation, rotation, and scaling along the normal direction at each point on the boundary.

Translation of the object can be represented via x and y translations τ^x and τ^y, respectively, as

$$\begin{pmatrix} \mathbf{x^c_{new}} \\ \mathbf{y^c_{new}} \end{pmatrix} = \begin{pmatrix} \mathbf{x^c_{old}} \\ \mathbf{y^c_{old}} \end{pmatrix} + \begin{pmatrix} \tau^x \mathbf{1} \\ \tau^y \mathbf{1} \end{pmatrix}, \tag{7}$$

where $\mathbf{1}$ is a column vector of ones of length N_{cent}, the number of RBF centers.

Object rotation is characterized by the rotation angle γ as

$$\begin{pmatrix} \mathbf{x}^{\mathbf{c}}_{\mathbf{new}} \\ \mathbf{y}^{\mathbf{c}}_{\mathbf{new}} \\ \boldsymbol{\theta}^{c}_{\mathrm{new}} \end{pmatrix} = \begin{pmatrix} \cos\gamma\mathbf{I} & \sin\gamma\mathbf{I} & \mathbf{O} \\ -\sin\gamma\mathbf{I} & \cos\gamma\mathbf{I} & \mathbf{O} \\ \mathbf{O} & \mathbf{O} & \mathbf{I} \end{pmatrix} \begin{pmatrix} \mathbf{x}^{\mathbf{c}}_{\mathbf{old}} \\ \mathbf{y}^{\mathbf{c}}_{\mathbf{old}} \\ \boldsymbol{\theta}^{c}_{\mathrm{old}} \end{pmatrix} + \begin{pmatrix} \mathbf{0} \\ \mathbf{0} \\ \gamma\mathbf{1} \end{pmatrix}, \tag{8}$$

where $\mathbf{I}$ and $\mathbf{O}$ are the N_{cent}-dimensional identity and zero matrices, respectively, and $\mathbf{0}$ is the N_{cent} long column vector of zeros.

Scaling along the normal at the boundary points can be represented as

$$\begin{pmatrix} \mathbf{x}^{\mathbf{c}}_{\mathbf{new}} \\ \mathbf{y}^{\mathbf{c}}_{\mathbf{new}} \end{pmatrix} = \begin{pmatrix} \mathbf{x}^{\mathbf{c}}_{\mathbf{old}} \\ \mathbf{y}^{\mathbf{c}}_{\mathbf{old}} \end{pmatrix} + \begin{pmatrix} \boldsymbol{\beta}^{\mathrm{diag}} \cos\boldsymbol{\theta}_{\mathrm{old}} \\ \boldsymbol{\beta}^{\mathrm{diag}} \sin\boldsymbol{\theta}_{\mathrm{old}} \end{pmatrix}, \tag{9}$$

where $\boldsymbol{\beta}^{\mathrm{diag}} := \mathrm{diag}(\beta^c(1)\ldots\beta^c(N_{\mathrm{cent}}))$ is the diagonal matrix of scaling factors corresponding to the boundary centers.

Thus we define the unknown to be reconstructed as

$$\mathbf{h} = (\alpha, (\mathbf{x}^{\mathbf{c}})^T, (\mathbf{z}^{\mathbf{c}})^T, (\boldsymbol{\theta}^{c})^T, (\boldsymbol{\beta}^{c})^T, \tau^x, \tau^y, \gamma, \mathbf{b}^{\mathbf{T}}, (\mathbf{t}^{\mathbf{x}})^T, (\mathbf{t}^{\mathbf{y}})^T, \mathbf{c}^{\mathbf{T}})^T, \tag{10}$$

where superscript "T" denotes matrix/vector transposition, and $\boldsymbol{\beta}^c$ is the vector (of the same size as either center-coordinate vector $\mathbf{x}^{\mathbf{c}}$ or $\mathbf{y}^{\mathbf{c}}$) representing the basic scaling factor along the normal direction at the boundary points corresponding to the RBF centers. τ^x (resp. τ^y) is the basic translation along the x (resp. y) direction, and γ is the angle of rotation of the object. The vectors $\{\mathbf{b}, \mathbf{t_x}, \mathbf{t_y}, \mathbf{c}\}$ represent the coefficients of assumed autoregressive processes governing the time variation of $\{\boldsymbol{\beta}^c, \tau_x, \tau_y, \gamma\}$ as follows:

Denoting the vector of normal-scaling factors at a time k by $\boldsymbol{\beta}^c_k \equiv (\beta^c_{k+1}(1)\ldots\beta^c_{k+1}(N_{\mathrm{cent}})$, its propagation equation can be written for $k = 0\ldots N_{\mathrm{views}} - 1$ as

$$\boldsymbol{\beta}^c_{k+1} = b_k\boldsymbol{\beta}^c_k = b_k\ldots b_1\boldsymbol{\beta}^c_0 \equiv \tilde{b}_k\boldsymbol{\beta}^c_0. \tag{11}$$

Similarly, for $k = 0\ldots N_{\mathrm{views}} - 1$, the translation of the object along the x or y direction is expressed as

$$\tau^p_{k+1} = t^p_k\tau^p_k = t^p_k\ldots t^p_1\tau^p_0, \tag{12}$$

where superscript p denotes either x or y.

The rotation angle propagates as

$$\gamma_{k+1} = e_k\gamma_k = e_k\ldots e_1\gamma_0. \tag{13}$$

We then denote $\mathbf{m} := [m_1\ldots m_{N_{\mathrm{views}}-1}]^T$, for $m = b, t^x, t^y, e$ in turn.

Thus, combining the actions of translation, rotation, and normal scaling, the RBF-center coordinates propagate as

$$\begin{pmatrix} \mathbf{x_{k+1}} \\ \mathbf{y_{k+1}} \end{pmatrix} = \begin{pmatrix} \mathbf{x_k}\cos\gamma_k + \mathbf{y_k}\sin\gamma_k \\ -\mathbf{x_k}\sin\gamma_k + \mathbf{y_k}\cos\gamma_k \end{pmatrix} + \begin{pmatrix} \tau^x_k \\ \tau^y_k \end{pmatrix} + \begin{pmatrix} \boldsymbol{\beta}^{\mathrm{diag}}_k \cos(\boldsymbol{\theta}_k + \gamma_k) \\ \boldsymbol{\beta}^{\mathrm{diag}}_k \sin(\boldsymbol{\theta}_k + \gamma_k) \end{pmatrix}, \tag{14}$$

where $\boldsymbol{\beta}^{\mathrm{diag}}_k := \mathrm{diag}(\beta_k(1)\ldots\beta_k(N_{\mathrm{cent}}))$, and the earlier superscript "c" representing the RBF-center-related parameters is suppressed for ease of notation. On the RHS, the first term represents RBF-center-coordinate rotation, the second yields the translation of the rotated coordinates, and the third scales the rotated and translated center coordinates along the unit normal after taking the coordinate rotation through angle γ into account.

The angle corresponding to the boundary-normal direction at each RBF center propagates as

$$\boldsymbol{\theta}_{k+1} = \boldsymbol{\theta}_k + \gamma_k, \tag{15}$$

where γ_k denotes the angle of rotation of the object.

Thus from the above formulation, using the definition of the state vector to be estimated as in Eqs. (10) and (11)–(15), we can now symbolically write a state propagation equation as

$$\mathbf{h^{k+1}} \equiv f_k(\mathbf{h^k}) = f_k(f_{k-1}(\mathbf{h^{k-1}})) = (f_k \circ f_{k-1}\ldots\circ f_0)(\mathbf{h^0}), \tag{16}$$

where the transition maps $f_k(.)$ are appropriately defined, and $\mathbf{h^0}$ is the state corresponding to the first time instant. Note also that the first time instant (i.e., $k = 0$ instant) can without loss of generality be assumed to correspond to a first view.

Hence we can now write Eq. (1) for $i = 0\ldots N_{\mathrm{views}} - 1$ as

$$\mathbf{z_i} = \mathbf{g_i}[\mathbf{h^i}], \tag{17}$$

where $\mathbf{z_i} := (p_{L1}(t_i)\ldots p_{Lr}(t_i))^T$ is the vector of ray integrals corresponding to the rays $L_1\ldots L_r$ in a view, and $\mathbf{g_i}(.)$ represents the ray-integral operator at the ith time instant/view.

Define by $\boldsymbol{\zeta}(\mathbf{h^0})$ the vector of residuals denoting the difference between the measured and predicted ray-integral data as

$$\begin{aligned} \boldsymbol{\zeta}(\mathbf{h^0}) &\triangleq \begin{pmatrix} \mathbf{z_0} - \mathbf{g_0}(\mathbf{h^0}) \\ \mathbf{z_1} - \mathbf{g_1}(\mathbf{h^1}) \\ \vdots \\ \mathbf{z_{M-1}} - \mathbf{g_{M-1}}(\mathbf{h^{M-1}}) \end{pmatrix} \\ &= \begin{pmatrix} \mathbf{z_0} - \mathbf{g_0}[\mathbf{h^0}] \\ \mathbf{z_1} - \mathbf{g_1}[\mathbf{f_0}(\mathbf{h^0})] \\ \vdots \\ \mathbf{z_{M-1}} - \mathbf{g_{M-1}}[(\mathbf{f_{M-2}} \circ \ldots \circ \mathbf{f_0})(\mathbf{h^0})] \end{pmatrix}, \end{aligned} \tag{18}$$

where we have set $M := N_{\mathrm{views}}$ for brevity of notation.

Thus the reconstruction problem of interest to us is about minimizing this residual vector with respect to $\mathbf{h^0}$. As is common practice, this problem is approximated by the following Tikhonov regularized nonlinear μ-minimum norm problem:

$$\min_{\mathbf{h}} \frac{1}{2}(\|\boldsymbol{\zeta}(\mathbf{h})\|^2 + \eta^2\|\mathbf{h}-\boldsymbol{\mu}\|^2), \tag{19}$$

where η is a regularization parameter, and $\boldsymbol{\mu}$ is a known constant representing *a priori* information, which is typically taken to be the initial estimate of the iterative process (it can be changed within the iterative process to help stabilize the iterates).

In this work, the minimization problem given by Eq. (19) is solved by using an iteratively regularized Gauss–Newton method [14] that solves, at the current iterate $\mathbf{h}$,

$$\min_{\mathbf{p}} \left\| \begin{pmatrix} \mathbf{J}(\mathbf{h})\mathbf{p} + \boldsymbol{\zeta}(\mathbf{h}) \\ \eta(\mathbf{h}-\boldsymbol{\mu}+\mathbf{p}) \end{pmatrix} \right\|^2, \tag{20}$$

where the $M \times N$ matrix $\mathbf{J}(\mathbf{h})$ is the Jacobian matrix of the functional $\boldsymbol{\zeta}(\mathbf{h})$ with respect to $\mathbf{h}$, defined via a Taylor series expansion of the form

$$\boldsymbol{\zeta}(\mathbf{h}+\mathbf{p}) = \boldsymbol{\zeta}(\mathbf{h}) + \mathbf{J}(\mathbf{h})\mathbf{p} + \mathcal{O}(\|\mathbf{p}\|^2). \tag{21}$$

The termination criterion we have used is a relative one; i.e., we measure "how much" of the residual remains to minimize. The relative criterion is defined as

$$\epsilon_{\text{rel}} = \frac{\|\mathcal{P}_{J\text{aug}}\boldsymbol{\zeta}_{\text{aug}}\|}{\|\boldsymbol{\zeta}_{\text{aug}}\|}, \tag{22}$$

where $\mathcal{P}_{J\text{aug}}$ is the orthogonal projection onto the range space of $\mathbf{J}_{\text{aug}}$, and

$$\mathbf{J}_{\text{aug}} = \begin{pmatrix} \mathbf{J}(\mathbf{h}) \\ \eta\mathbf{I}_N \end{pmatrix}.$$

Termination of the nonlinear recursive scheme is set as satisfaction of the criterion $\epsilon_{\text{rel}} < \text{tol}$ for some tolerance limit "tol" or the iterates staying stable.

The GN scheme thus requires the computation of the Frechet derivatives of the measured ray integrals with respect to the parameter vector. This aspect is dealt with in the following section.

3. Dynamic Shape Derivatives

Define the residual vector at each time instant $i \in \{0,\ldots,M-1\}$ as

$$\mathbf{r_i} := \mathbf{z_i} - \mathbf{g_i}(\mathbf{h^i}) = \mathbf{z_i} - \mathbf{g_i}[(\mathbf{f_{i-1}} \circ \ldots \circ \mathbf{f_0})(\mathbf{h^0})]. \tag{23}$$

Thus the GN iteration would require the evaluation of a Jacobian matrix $\mathbf{J}$ evaluated as

$$\mathbf{J} \equiv \begin{pmatrix} \mathbf{J}_0 \\ \vdots \\ \mathbf{J}_{M-1} \end{pmatrix}, \tag{24}$$

where the ith submatrix of $\mathbf{J}$ corresponding to the ith residual is given by

$$\begin{aligned} \mathbf{J_i} := \frac{\partial \mathbf{r_i}}{\partial \mathbf{h^0}} &= -\mathbf{G_i}[\mathbf{h^i}]\mathbf{F_{i-1}}[\mathbf{h^{i-1}}]\ldots\mathbf{F_{i-i}}[\mathbf{h^{i-i}}] \\ &= -\mathbf{G_i}[\mathbf{h^i}]\mathbf{F_{i-1}}[\mathbf{h^{i-1}}]\ldots\mathbf{F_0}[\mathbf{h^0}], \end{aligned} \tag{25}$$

where, as defined earlier in Eq. (16),

$$\mathbf{h^i} = f_{i-1}(\mathbf{h^{i-1}})) = (f_i \circ f_{i-1} \ldots \circ f_0)(\mathbf{h^0}).$$

$\mathbf{G_i}[.]$ and $\mathbf{F_i}[.]$ are the Frechet derivatives of the measurement and state-transition operators at the ith view/time instant, respectively.

The Frechet derivative $\mathbf{F_i}[\mathbf{h^i}]$ corresponding to the state-transition operator $\mathbf{f_i}(\mathbf{h^i})$ is straightforwardly evaluated from Eq. (16) and is given in Appendix B for completeness.

Evaluation of the measurement-related derivatives as in $\mathbf{G_i}[\mathbf{h^i}]$ is typically accomplished by using the chain rule to combine a Frechet-derivative calculation with respect to the (discretized) pointwise unknowns together with the variation of the pointwise unknown with needed shape parameters as in [14] (and references therein). In our work, we propose a novel ray-tomographic scheme for evaluating the shape derivatives via continuous ray tracing, without needing to evaluate the pointwise derivatives via a discrete ray trace in a discretized object representation. Thus, we are using a single object representation in the ray-trace and Frechet-derivative parts of the forward problem.

Recall that the ray integral corresponding to a ray indexed as l at a time instant i is modeled as

$$z_l := \int_{\text{Ray } l} \alpha(x,y)\mathrm{d}s = \sum_{j=1}^{N_l} w_{lj}\alpha_{lj}, \tag{26}$$

where w_{lj} are appropriate quadrature weights, $\{\alpha_{lj}\}$ represent the values of the unknown inhomogeneity on the ray l at the quadrature points indexed by j, and N_l is the number of quadrature points on the lth ray, and the explicit presence of the time instant i in the equation above is omitted for ease of notation.

Defining $\mathbf{w}_l = (w_{l1}\ldots w_{lN_l})^T$, and, $\alpha_l = (\alpha_{l1}\ldots\alpha_{lN_i})$, we can write

$$z_l = \mathbf{w}_l^T\alpha_l. \tag{27}$$

Further, since we have assumed the form $\alpha(\mathbf{r},t) = \alpha_0 H_\rho[s(\mathbf{r},t)]$, we have for a given time instant

$$\alpha_{lj} = \alpha_0 H_\rho[s_{lj}], \tag{28}$$

where $s_{lj} = s(\mathbf{r}_j^l)$, with $\mathbf{r}_j^l = (x_j^l, y_j^l)$ being the jth quadrature point of the lth ray.

Hence, we can write

$$z_l = \mathbf{w}_l^T \alpha_0 H_\rho[\mathbf{s_l}], \tag{29}$$

where $\mathbf{s_l} := (s_{l1} \ldots s_{lN_l})^T$.

Thus, the first variation of the measurements with respect to the level-set values can be expressed as

$$\delta z_l = \mathbf{w}_l^T H_\rho[\mathbf{s}_l]\delta\alpha_0 + \alpha_0 \mathbf{w}_l^T \mathrm{diag}(H'_\rho[\mathbf{s}_l])\delta\mathbf{s}_l \tag{30}$$

$$= \mathbf{w}_l^T H_\rho[\mathbf{s}_l]\delta\alpha_0 + \alpha_0 \mathbf{w}_l^T \mathrm{diag}(H'_\rho[\mathbf{s}_l])\mathbf{J}_l \begin{pmatrix} \delta\mathbf{x} \\ \delta\mathbf{y} \\ \delta\boldsymbol{\theta} \end{pmatrix} \tag{31}$$

$$\equiv \nabla\mathbf{g}_l^T \delta\tilde{\mathbf{h}}, \tag{32}$$

where,

$$\nabla\mathbf{g}_l = (\mathbf{w}_l^T H_\rho[\mathbf{s}_l]\delta\alpha_0 + \alpha_0 \mathbf{w}_l^T \mathrm{diag}(H'_\rho[\mathbf{s}_l])\mathbf{J}_l)^T \tag{33}$$

and $\delta\tilde{\mathbf{h}} = (\delta\alpha_0 \delta\mathbf{x}^T \delta\mathbf{y}^T \delta\boldsymbol{\theta}^T)^T$, in which $\delta\mathbf{s}_l$ is the first variation of the level-set values on the line l with respect to the variation in center parameters $\{\delta\mathbf{x}, \delta\mathbf{y}, \delta\boldsymbol{\theta}\}$ at the time instant considered, and the matrix $\mathbf{J}_l$ is the corresponding Jacobian matrix that is calculated in [17] and given in Appendix A for completeness.

Note that the vector $H'_\rho[\mathbf{s}_l]$ has very few nonzero values since the derivative $H'(.)$ of the approximate Heaviside has a small support. This results in the Jacobian matrix corresponding to the lth ray having to be computed for very few points on the ray that are in a tube close to the boundary.

Combining all the ray integrals that are available at the time instant i, we have

$$\mathbf{G_i} = (\nabla\mathbf{g}_{i1} \ldots \nabla\mathbf{g}_{iL})^T, \tag{34}$$

where $\nabla\mathbf{g}_{il}$ denotes the gradient corresponding to the lth ray-integral at the ith time instant.

The above evaluation of the Frechet derivatives does not need to evaluate the pointwise Jacobian (which is nothing but the ray-path matrix in this case [24]), thus removing any inconsistency that would otherwise be there between the shape-based representation and a grid-based interpolation for computing the pointwise derivatives.

A note on the Heaviside approximation: we observe from Eq. (3) that the support of $H'_\rho[s(\mathbf{r})]$ is contained in $s^{-1}[-\rho, \rho]$. The choice of the Heaviside parameter ρ should be such that the interpolating function $s(\mathbf{r})$ should be a good approximation to a signed distance function in the "tubular" region $s^{-1}[-\rho, \rho]$. In our work, as in [14], for a plane curve $\gamma(x, y) = 0$ such as in the two-dimensional problems under consideration, we can define the tube as consisting of all parallel curves $\tilde{s}(x, y) = \varepsilon$ such that $|\varepsilon\kappa(x, y)| < 1$ for all values of $(x, y) \in \partial\Omega$, where $\kappa(x, y)$ is the curvature of the curve $\tilde{s}(x, y) = 0$. This condition ensures that a parallel curve is regular, as well as that the normal vectors of the curve $\tilde{s}(x, y) = 0$ coincide with those of a parallel curve $\tilde{s}(x, y) = \varepsilon$ for all $(x, y) \in \partial\Omega$ [25,26].

4. Numerical Studies

A. Case Studies and Methodology

We validate our formulations by reconstructions of a time-varying phantom with two different assumed state-variable models. The data are obtained for one view at each time instant, with the object undergoing geometric transformations in between. The transformations we consider are (x and y) translation, rotation, and pointwise-normal scaling. The corresponding parameters [as in Eq. (10)] characterizing these transformations are τ^x and τ^y for x and y translations, respectively, γ for rotation, and β for pointwise-normal scaling. In our reconstructions, we have used the triharmonic basic function, i.e., $\Phi(\mathbf{r}) = r^4 \ln r$, with a quadratic polynomial basis.

In our first state model (denoted as SM-1), we consider the translation, rotation, and scaling parameters fixed across views; i.e., they propagate with autoregressive coefficients [Eqs. (11)–(13)] of unity. In addition, the pointwise-normal scaling parameter β is considered fixed for all boundary points. The second state model (denoted as SM-2) considers the same three transformations with the corresponding parameters governing them taking different values at each view; in addition the pointwise-normal scaling parameter β takes a different value at each boundary point.

We have considered reconstruction of an object with unknown refractive-index difference to be −0.02, from 20 views and 40 rays per view. At each time instant ray-integral data are obtained for a view and the object is assumed to be geometrically transforming in the duration between the measurement time instants. In principle, the number of centers can be considered as an implicit regularization parameter in the solution of the reconstruction problem; however, for the numerical studies in this work we fix this *a priori* and regularize the resultant almost rank-deficient problem in the iterative regularization scheme. In our present studies, we typically picked the minimum number of RBF centers that yielded closed curves for the reconstructions considered across all models considered; we chose eight centers for our reconstructions.

The ray-integral data are generated via continuous ray tracing [27] followed by the addition of zero-mean Gaussian noise.

The Gauss–Newton scheme used in the reconstructions is summarized in the chart below:

I. *Initialization*

(a) Set the initial estimate $\mathbf{h}^0$.
(b) $\boldsymbol{\mu} = \mathbf{h}^0$, η set at a suitable "large" value.

II. *Reconstruction phase*

For $k = 1, 2, \ldots$, until $\epsilon_{\text{rel}} < \text{tol}$ or residual is unchanging for many past k:

(a) Estimate the Heaviside approximation parameter, ρ, as $\min(dl, \varepsilon_{\max})$, where $\varepsilon_{\max} = \max\{\varepsilon; |\varepsilon\kappa(x,y)| < 1 \text{ for all values of } (x,y) \in \partial\Omega\}$ and dl is the ray-integral-discretization interval.

(b) Evaluate the Jacobian $\mathbf{J}(\mathbf{h}^k)$ using Eq. (24).

(c) Solve Eq. (20) for $\mathbf{p}^k$.

(d) Do a line search to find step-length σ_k.

(e) If $\beta_k \simeq 1$, then $\eta := \eta/q$, for a suitable choice of $q > 1$ (we chose $q = 2$).

(f) $\mathbf{h}^{k+1} = \mathbf{h}^k + \sigma_k \mathbf{p}^k$.

In order to incorporate bound constraints, in the optimization steps we use a projected gradient update [28].

B. Discussion and Quantification of Results

In this subsection, we analyze the reconstructions obtained with the aid of a quantification of the quality of reconstructions via three error measures with respect to the optical parameter, the area-parameter product, and the centroid of the object.

Reconstructions are shown for a concave phantom with different noise levels for each of these state models. Results are also shown for a convex elliptical phantom with the SM-2 model. In addition, results are presented using SM-2 based reconstructions on data obtained from SM-1 transitions; this set of results corresponds to an "overfit" of parameters in the reconstructions, in that only a few of the reconstructed parameters are involved in the actual data creation.

The reconstructions obtained for the cases mentioned above are plotted in Figs. 1–4, and are seen to show good agreement between the reconstructed and actual shapes. Also, the refractive-index difference is well reconstructed.

While we observe in Fig. 1 (SM-1 reconstructions) that the concave part of the phantom is sometimes not estimated accurately, the issue might be hypothesized to be a data-noise-related local minimum of the objective function that is overestimating the present concavity. We performed the reconstructions with seven and eight centers for the SM-1 zero-noise data, and these are found to be almost exact, thus giving a justification for the above hypothesis. These "noiseless" reconstructions are given in Fig. 5 for eight centers. Of course, the local minimum issue need not be only noise-related as our experience with other noiseless data sets point out, where even though the reconstructions are as expected tracking the shape better than with noisy data, there are mild locational discrepancies.

We point out, however, that the reconstructions with noisy data are quite close to the actual phantoms—visually as well as quantitatively (as will be defined below)—indicating that the present algorithm performs well.

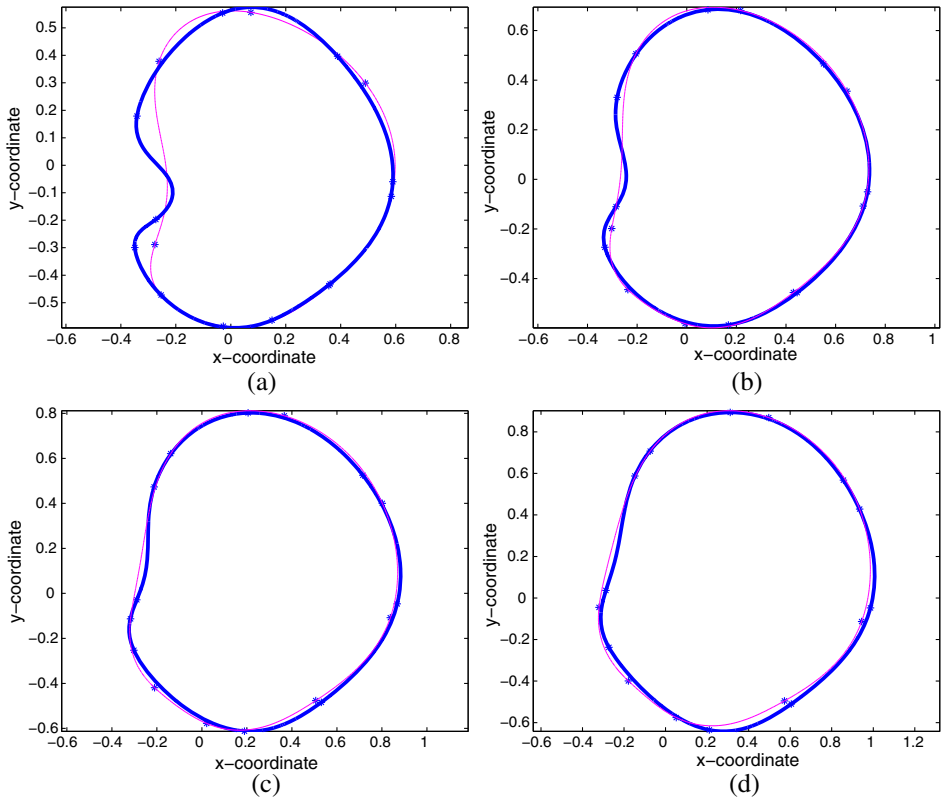

Fig. 1. SM-1 reconstructions (thick and thin lines show the reconstruction and actual object, respectively) obtained for a concave phantom from data with SNR = 16.4 dB corresponding to (a) first view, (b) seventh view, (c) 14th view, and (d) 20th view. Reconstructed, $\alpha = -0.01989$; actual, $\alpha = -0.0200$.

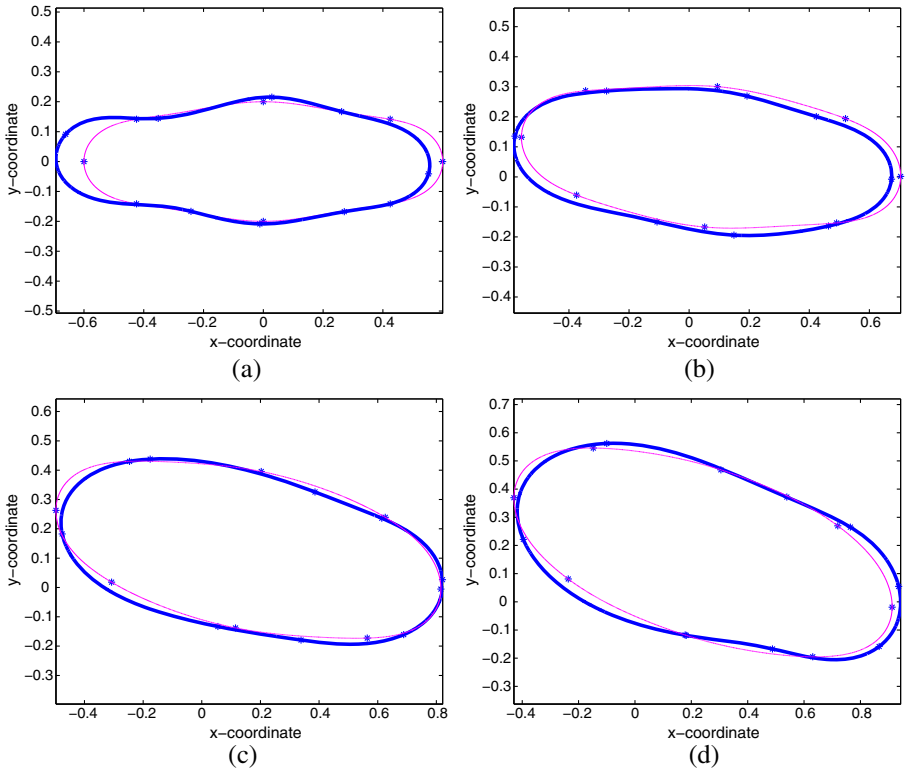

Fig. 2. SM-2 reconstructions (thick and thin lines show the reconstruction and actual object, respectively) for an elliptical phantom obtained from data with SNR = 11.574 dB corresponding to (a) first view, (b) seventh view, (c) 14th view, and (d) 20th view. Reconstructed, $\alpha = -0.01956$; actual, $\alpha = -0.0200$.

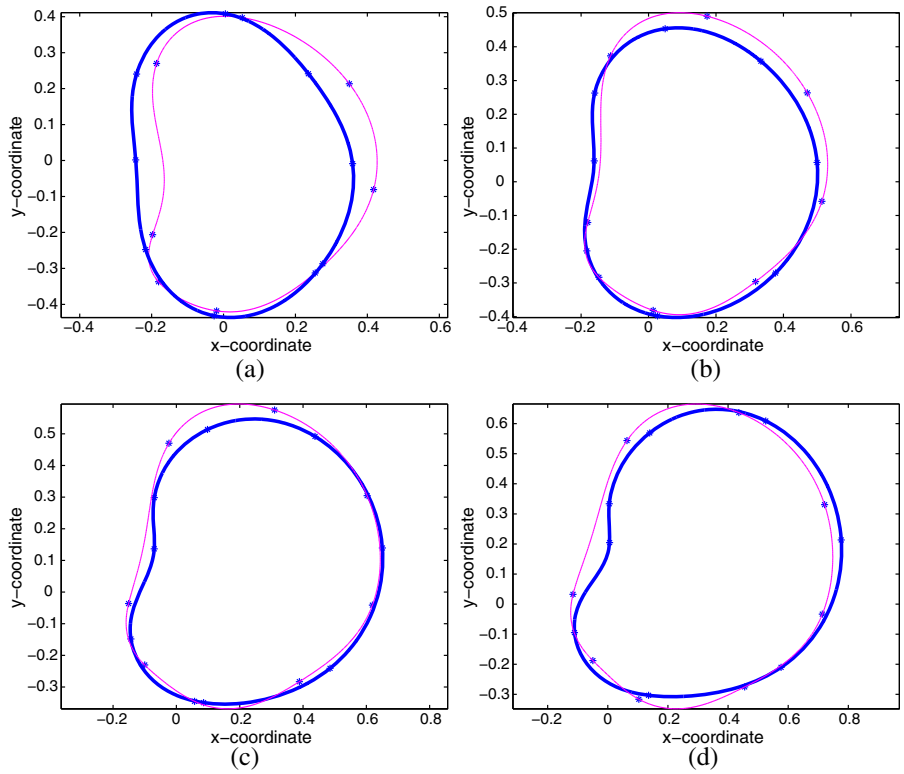

Fig. 3. SM-2 reconstructions (thick and thin lines show the reconstruction and actual object, respectively) obtained for a concave phantom from data with SNR = 11.393 dB corresponding to (a) first view, (b) seventh view, (c) 14th view, and (d) 20th view. Reconstructed, $\alpha = -0.0210$; actual, $\alpha = -0.0200$.

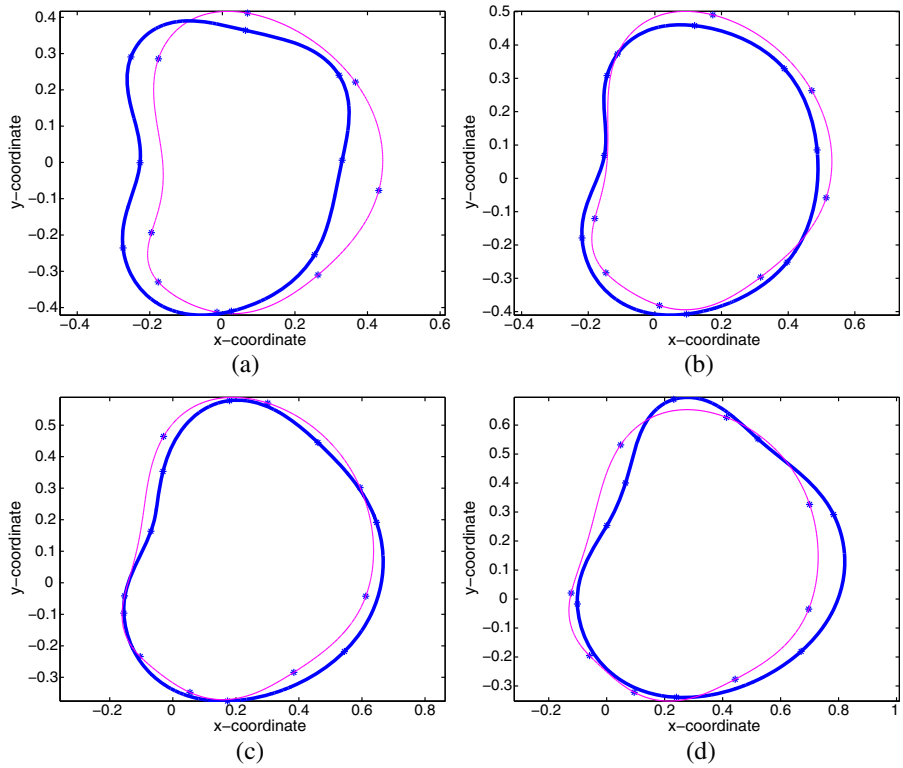

Fig. 4. SM-2 reconstructions (thick and thin lines show the reconstruction and actual object, respectively) obtained for a concave phantom from SM-1 data with SNR = 11.434 dB corresponding to (a) first view, (b) seventh view, (c) 14th view, and (d) 20th view. Reconstructed, $\alpha = -0.01989$; actual, $\alpha = -0.0200$.

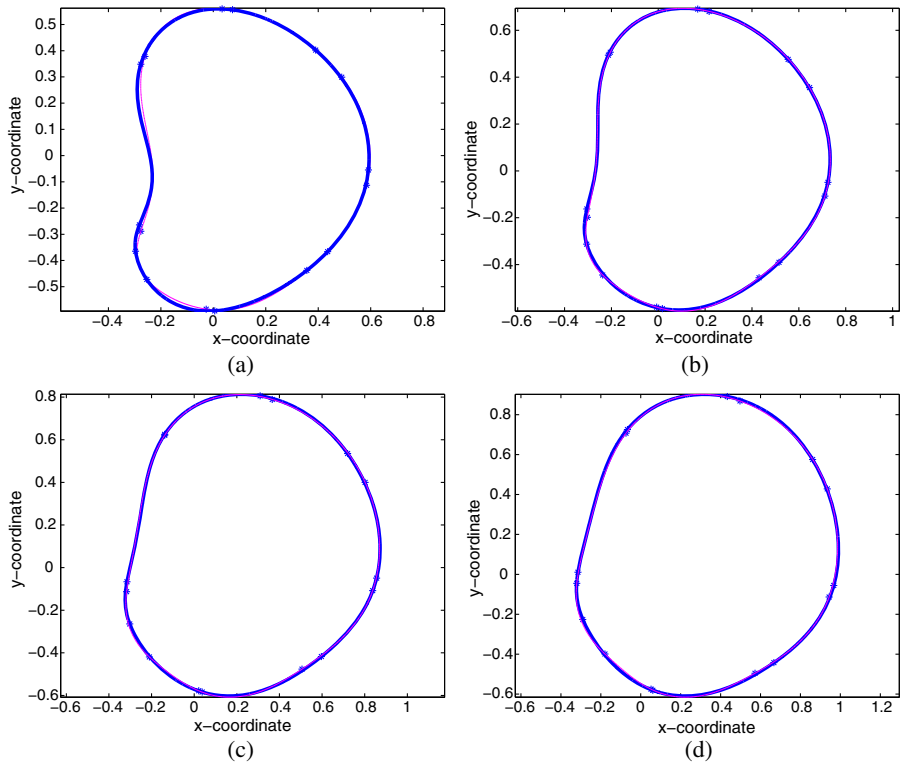

Fig. 5. SM-1 reconstructions (thick and thin lines show the reconstruction and actual object, respectively) obtained for a concave phantom from noiseless data corresponding to (a) first view, (b) seventh view, (c) 14th view, and (d) 20th view. Reconstructed, $\alpha = -0.01996$; actual, $\alpha = -0.0200$.

In order to quantify the quality of reconstructions we utilize three error measures, namely, a normalized percentage of error of the area-parameter product [parameter here referring to the optical parameter of refractive-index difference (w.r.t the background) α], a normalized percentage of error of the refractive-index difference, and the distance of the centroid of the reconstructed object from its actual position.

We define an area-parameter-product error measure as

$$E_a = \frac{|\alpha_{\text{rec}} A_{\text{rec}} - \alpha_{ac} A_{ac}|}{|\alpha_{ac} A_{ac}|} \times 100, \tag{35}$$

where α_{rec} and α_{ac} are the reconstructed and actual values of the optical parameter, respectively, and A_{rec} and A_{ac} are the reconstructed and actual values of the area of the object, respectively.

An error measure of the difference between the actual and reconstructed refractive-index differences is defined as

$$E_\alpha = \frac{|\alpha_{\text{rec}} - \alpha_{ac}|}{|\alpha_{ac}|} \times 100. \tag{36}$$

The Euclidean distance

$$E_c = \sqrt{(\bar{x}_{\text{rec}} - \bar{x}_{ac})^2 + (\bar{y}_{\text{rec}} - \bar{y}_{ac})^2}, \tag{37}$$

between the centroids of the reconstructed and actual objects, is another error measure that quantifies the reconstruction. Here, $(\bar{x}_{\text{rec}}, \bar{y}_{\text{rec}})$ (resp. $(\bar{x}_{ac}, \bar{y}_{ac})$) are the centroid coordinates for the reconstructed (resp. actual) object.

The area and centroid coordinates are evaluated by discretizing the reconstructed/actual images, and are defined as

$$A_{\text{object}} = \sum_{i,j} \chi_{\text{object}}(x_i, y_j), \tag{38}$$

$$\bar{x}_{\text{object}} = \frac{\sum_{i,j} x_i \chi_{\text{object}}(x_i, y_j)}{A_{\text{object}}}, \tag{39}$$

$$\bar{y}_{\text{object}} = \frac{\sum_{i,j} y_i \chi_{\text{object}}(x_i, y_j)}{A_{\text{object}}}, \tag{40}$$

where the indices (i,j) range over the extent of the discretized image, and $\chi_{\text{object}}(.)$ is the characteristic function with respect to the object support.

We take these error measures as the average errors across all views/time instants at which measurements are collected; the results are tabulated in Table 1, along with the reconstructed and actual values of the refractive-index parameter. The small errors obtained show the basic efficacy of the proposed scheme. The relatively larger shape errors obtained in the "overfitting" case-4 (in Table 1) point out that the choice of an appropriate model is important to obtain good reconstructions. Similarly, as mentioned above, the choice of the number of centers is also of importance since that number acts as another implicit regularization parameter. The development of adaptive schemes to address these aspects of model appropriateness is an important direction of future work.

Table 1. Error Measures for Reconstructions[a]

Phantom	DM	RM	E_α%	E_a%	E_c
Concave	SM-1	SM-1	0.541	0.997	0.01
Ellipse	SM-2	SM-2	2.205	1.531	0.024
Concave	SM-2	SM-2	5.483	1.548	0.031
Concave	SM-1	SM-2	0.507	1.653	0.044
Concave (noiseless)	SM-1	SM-1	0.201	0.202	0.001

[a]DM and RM denote the data model and reconstruction model, respectively. E_α, E_a, and E_c denote the parameter, area-parameter-product, and centroid error measures, respectively.

5. Conclusions

In this paper, with the objective of reconstructing time-varying geometrically deforming features of interest, a novel level-set-based reconstruction scheme for ray tomography is proposed for shape and electromagnetic parameters using a regularized Gauss–Newton-filter-based scheme. We use an implicit Hermite-interpolation-based RBF representation of the zero level set corresponding to the boundary curve. Numerical results validating the formulation are presented for a straight ray-based tomographic reconstruction.

The contribution of our present work is to set up the framework for the time-varying shape-reconstruction problem with unknown dynamics in an RBF-based level-set parametrization with respect to a regularized Gauss–Newton-filter scheme. In addition, we assume the class of shape transitions to be of a nonlinear kind, consisting of the affine class in addition to a pointwise-normal scaling. Another important contribution of the paper is an evaluation of the shape-related Frechet derivatives that does not need to evaluate the pointwise Jacobian (the ray-path matrix in our ray-tomography problem).

The Gauss–Newton filter [21] is a batch estimator of time-varying states and overcomes to quite an extent the tuning issues of nonlinear Kalman filtering. Also, scaling along the normal at a boundary point is a deformation that is natural with respect to level-set schemes since only boundary perturbations along the normal are considered in these. This "naturalness" of normal deformations is emphasized in the case of the Hermite-RBF-interpolation-based representations, since the normals at the RBF centers are reconstructed along with the center coordinates. To the best of our knowledge, this paper presents the first tomographic reconstruction results in these settings.

Appendix A: RBF Interpolation Matrix and Level-Set Derivative

1. RBF Interpolation Matrix

Applying the interpolation conditions Eq. (4) to the assumed form of the interpolating function Eq. (5), we obtain the RBF Hermite interpolation problem in matrix form:

$$\begin{bmatrix} A & P \\ P^T & O \end{bmatrix}\begin{bmatrix} \lambda \\ \mathbf{a} \end{bmatrix} = \begin{bmatrix} \mathbf{b} \\ 0 \end{bmatrix}, \tag{A1}$$

with the entries $A_{ij} = \mu_i^{\mathbf{r}}\mu_j^{\mathbf{t}}\Phi(\mathbf{r}-\mathbf{t})$, $P_{ij} = \mu_i(p_j)$, where $p(\mathbf{r}) = \sum_{l=1}^{L} a_l p_l(\mathbf{r})$ for some basis $\{p_1, \ldots, p_\ell\}$ for the space π_{k-1}^d, and $\boldsymbol{\lambda} \equiv \binom{\mathbf{c}}{\mathbf{d}}$. The expressions for the entries in the matrices A and P of Eq. (A1) are now given below. First,

$$P_{ij} = \mu_i(p_j) = \begin{cases} p_j(\mathbf{r}_i^c), & 1 \le i \le m, \\ \mathbf{n}_i \cdot \nabla p_j(\mathbf{r}_{i-m}^c), & m+1 \le i \le 2m. \end{cases} \tag{A2}$$

Furthermore $A_{ij} = \mu_i^{\mathbf{r}}\mu_j^{\mathbf{t}}\Phi(\mathbf{r}-\mathbf{t})$, which implies

$$A_{ij} = \begin{cases} \Phi(\mathbf{r}-\mathbf{r}_j^c), & \text{if } 1 \le i,j \le m, \\ -\mathbf{n}_{j-m} \cdot (\nabla\Phi)(\mathbf{r}_i^c - \mathbf{r}_{j-m}^c), & \text{if } 1 \le i \le m, \quad \text{and} \quad m+1 \le j \le 2m, \\ \mathbf{n}_{i-m} \cdot (\nabla\Phi)(\mathbf{r}_{i-m}^c - \mathbf{r}_j^c), & \text{if } m+1 \le i \le 2m, \quad \text{and} \quad 1 \le j \le m, \\ -\mathbf{n}_{i-m}^T H(\mathbf{r}_{i-m} - \mathbf{r}_{j-m})\mathbf{n}_{j-m}, & \text{if } m+1 \le i,j \le 2m, \end{cases} \tag{A3}$$

where $H(\mathbf{r})$ is the $d \times d$ Hessian matrix with $h_{k\ell} = (\partial^2/\partial x_k \partial x_\ell)\Phi$. Thus we can write the matrix A in $m \times m$ block form as $A = \binom{A^{(11)}\ A^{(12)}}{A^{(21)}\ A^{(22)}}$.

2. Level-Set Derivative

In this part of the appendix, for the sake of completeness, following [17], we write the first variation of the level-set values with respect to those of the RBF-center coordinates and normals that are used in Eq. (30) for the shape derivatives.

We now recall from Eq. (5) that

$$s(\mathbf{r}) = \sum_{l=1}^{L} a_l p_l(\mathbf{r}) + \sum_{j=1}^{m}[c_j\Phi(\mathbf{r}-\mathbf{r}_j^c) - d_j\Psi_j(\mathbf{r}-\mathbf{r}_j^c)], \tag{A4}$$

where $\Psi_j(.) \equiv (D_{n_j}\Phi)(.)$, and

$$\begin{aligned}\Psi_j(\mathbf{r}-\mathbf{r}_j^c) &\equiv (\nabla\phi)(\mathbf{r}-\mathbf{r}_j^c)\cdot\mathbf{n}_j \\ &= \phi_x(\mathbf{r}-\mathbf{r}_j^c)\mathrm{Cos}\theta_j^c + \phi_y(\mathbf{r}-\mathbf{r}_j^c)\mathrm{Sin}\theta_j^c\end{aligned} \tag{A5}$$

Evaluating the first variation of s, we have

$$\begin{aligned}\delta s(\mathbf{r}) = \sum_{l=1}^{L}\delta a_l p_l(\mathbf{r}) + \sum_{j=1}^{m}[&c_j\delta\Phi(\mathbf{r}-\mathbf{r}_j^c) + \delta c_j\Phi(\mathbf{r}-\mathbf{r}_j^c) \\ &- d_j\delta\Psi_j(\mathbf{r}-\mathbf{r}_j^c) - \delta d_j\Psi_j(\mathbf{r}-\mathbf{r}_j^c)],\end{aligned} \tag{A6}$$

where, further,

$$\delta\Phi(\mathbf{r}-\mathbf{r}_j^c) = -\Phi_x(\mathbf{r}-\mathbf{r}_j^c)\delta x_j^c - \Phi_y(\mathbf{r}-\mathbf{r}_j^c)\delta y_j^c \tag{A7}$$

and similarly,

$$\delta\Psi_j(\mathbf{r}-\mathbf{r}_j^c) = [-\Phi_{xx}(\mathbf{r}-\mathbf{r}_j^c)\mathrm{Cos}\theta_j^c - \Phi_{yx}(\mathbf{r}-\mathbf{r}_j^c)\mathrm{Sin}\theta_j^c]\delta x_j^c \tag{A8}$$

$$+[-\Phi_{xy}(\mathbf{r}-\mathbf{r}_j^c)\mathrm{Cos}\theta_j^c - \Phi_{yy}(\mathbf{r}-\mathbf{r}_j^c)\mathrm{Sin}\theta_j^c]\delta y_j^c \tag{A9}$$

$$+[-\Phi_x(\mathbf{r}-\mathbf{r}_j^c)\mathrm{Sin}\theta_j^c + \Phi_y(\mathbf{r}-\mathbf{r}_j^c)]\delta\theta_j^c. \tag{A10}$$

Hence, in Eq. (A6), it only remains to evaluate δc_j and δd_j in terms of the variations of the RBF centers and normals, i.e., to evaluate $\delta\boldsymbol{\lambda}$ and $\delta\mathbf{a}$. To do this, we take the first variation of the interpolation system of Eq. (A1) to obtain

$$\begin{pmatrix} \delta A & \delta P \\ \delta P^T & \mathbf{0} \end{pmatrix}\begin{pmatrix} \boldsymbol{\lambda} \\ \mathbf{a} \end{pmatrix} + \begin{pmatrix} A & P \\ P^T & \mathbf{0} \end{pmatrix}\begin{pmatrix} \delta\boldsymbol{\lambda} \\ \delta\mathbf{a} \end{pmatrix} = \mathbf{0}. \tag{A11}$$

Hence we obtain

$$\begin{pmatrix} \delta\boldsymbol{\lambda} \\ \delta\mathbf{a} \end{pmatrix} = -\begin{pmatrix} A & P \\ P^T & \mathbf{0} \end{pmatrix}^{-1}\begin{pmatrix} (\delta A)\boldsymbol{\lambda} + (\delta P)\mathbf{a} \\ (\delta P^T)\boldsymbol{\lambda} \end{pmatrix}. \tag{A12}$$

We now make the following definitions:

$$(\delta A)\boldsymbol{\lambda} \equiv B\begin{pmatrix} \delta\mathbf{x}^{\mathbf{c}} \\ \delta\mathbf{y}^{\mathbf{c}} \\ \delta\theta^{\mathbf{c}} \end{pmatrix}, \qquad (\delta P)\mathbf{a} \equiv P_a\begin{pmatrix} \delta\mathbf{x}^{\mathbf{c}} \\ \delta\mathbf{y}^{\mathbf{c}} \\ \delta\theta^{\mathbf{c}} \end{pmatrix},$$

$$(\delta P^T)\boldsymbol{\lambda} \equiv P_\lambda\begin{pmatrix} \delta\mathbf{x}^{\mathbf{c}} \\ \delta\mathbf{y}^{\mathbf{c}} \\ \delta\theta^{\mathbf{c}} \end{pmatrix}, \tag{A13}$$

where the functional forms (explicitly given in Appendix A of [17]) for B, P_a, and P_λ are obtained by appropriate rearrangement of the respective left-hand sides in the expressions above.

Considering $\mathbf{s}$ to be the vector of values of $s(\mathbf{r})$ at the required (N_T number of) points in a tube of radius ρ about the boundary, we can thus write [17]

$$\delta\mathbf{s} = \mathbf{J}_s \begin{pmatrix} \delta\mathbf{x^c} \\ \delta\mathbf{y^c} \\ \delta\theta^{\mathbf{c}} \end{pmatrix}, \tag{A14}$$

where

$$\mathbf{J}_s = F - (R[\tilde{A}^{-1}]_a + \Phi[\tilde{A}^{-1}]_c - \Psi[\tilde{A}^{-1}]_d)\tilde{B}, \tag{A15}$$

where again,

1. $\tilde{A} \equiv \begin{pmatrix} A & P \\ P^T & \mathbf{0} \end{pmatrix}$, and $\tilde{B} \equiv \begin{pmatrix} B+P_a \\ P_\lambda \end{pmatrix}$.
2. $\mathbf{\Phi}$ (resp. $\mathbf{\Psi}$) is the $N_T \times m$ matrix with $\mathbf{\Phi}_{ij} = \Phi(\mathbf{r}_i - \mathbf{r}_j^c)$ (resp. $\mathbf{\Psi}_{ij} = \Psi_j(\mathbf{r}_i - \mathbf{r}_j^c)$), where $\mathbf{r}_i$ is the i th point at which the value of δs needs to be calculated. Similarly, the derivative matrices $\mathbf{\Phi}_x$, $\mathbf{\Phi}_y$, $\mathbf{\Phi}_{xx}$, $\mathbf{\Phi}_{xy}$, and $\mathbf{\Phi}_{yy}$ can be defined.
3. R is an $N_T \times L$ matrix with $R_{nl} = p_l(\mathbf{r}_n)$.
4. $[\tilde{A}^{-1}]_a$ (resp. $[\tilde{A}^{-1}]_c$ and $[\tilde{A}^{-1}]_d$) corresponds to the last L rows (resp. rows 1 to m and $m+1$ to $2m$) of $\tilde{A}^{-1}$.
5. $F = [F^x F^y F^\theta]$, with

$$F^x = -\mathbf{\Phi}_x\Lambda(\mathbf{c}) + [\mathbf{\Phi}_{xx}\Lambda(\mathrm{Cos}\boldsymbol{\theta}^c) + \mathbf{\Phi}_{yx}\Lambda(\mathrm{Sin}\boldsymbol{\theta}^c)]\Lambda(\mathbf{d}), \tag{A16}$$

$$F^y = -\mathbf{\Phi}_y\Lambda(\mathbf{c}) + [\mathbf{\Phi}_{xy}\Lambda(\mathrm{Cos}\,\boldsymbol{\theta}^c) + \mathbf{\Phi}_{yy}\Lambda(\mathrm{Sin}\,\boldsymbol{\theta}^c)]\Lambda(\mathbf{d}), \tag{A17}$$

$$F^\theta = [\mathbf{\Phi}_x\Lambda(\mathrm{Sin}\,\boldsymbol{\theta}^c) - \mathbf{\Phi}_y\Lambda(\mathrm{Cos}\boldsymbol{\theta}^c)]\Lambda(\mathbf{d}), \tag{A18}$$

where $\Lambda(\mathbf{v}) \equiv \mathrm{diag}(v_1 \ldots v_m)$ for some vector $\mathbf{v}$.

Appendix B: Transition Jacobian

In this appendix, we write out the Jacobian matrix corresponding to the state-transition model Eq. (16) considered in our work. The Jacobian matrix $\mathbf{F_i}[\mathbf{h_i}]$ (denoted in short form as $\mathbf{F_i}$) evaluated at a nominal $\mathbf{h_i}$ corresponding to the i th time instant is detailed below:

$$\mathbf{F_i} \equiv \begin{pmatrix} 1 & \mathbf{0}_C^T & \mathbf{0}_C^T & \mathbf{0}_C^T & \mathbf{0}_C^T & 0 & 0 & 0 & \mathbf{O}_{C,P} \\ \mathbf{0}_C & \cos\gamma\mathbf{I}_C & \sin\gamma\mathbf{I}_C & -[\boldsymbol{\beta}][\sin\boldsymbol{\varepsilon}] & [\cos\boldsymbol{\varepsilon}] & \mathbf{1}_C & \mathbf{0}_C & -\boldsymbol{\beta}.*\sin\boldsymbol{\varepsilon} + (-\mathbf{x}\sin\gamma + \mathbf{y}\cos\gamma) & \mathbf{O}_{C,P} \\ \mathbf{0}_C & -\sin\gamma\mathbf{I}_C & \cos\gamma\mathbf{I}_C & [\boldsymbol{\beta}][\cos\boldsymbol{\varepsilon}] & [\sin\boldsymbol{\varepsilon}] & \mathbf{0}_C & \mathbf{1}_C & (\boldsymbol{\beta}.*\cos\boldsymbol{\varepsilon} - (\mathbf{x}\cos\gamma + \mathbf{y}\sin\gamma)) & \mathbf{O}_{C,P} \\ \mathbf{0}_C & \mathbf{O}_{C,C} & \mathbf{O}_{C,C} & \mathbf{I}_C & \mathbf{O}_{C,C} & \mathbf{0}_C & \mathbf{0}_C & \mathbf{1}_C & \mathbf{O}_{C,P} \\ \mathbf{0}_C & \mathbf{O}_{C,C} & \mathbf{O}_{C,C} & \mathbf{O}_{C,C} & b_{i-1}\mathbf{I}_C & \mathbf{0}_C & \mathbf{0}_C & \mathbf{0}_C & (\boldsymbol{\beta}\mathbf{u_i}^T|\mathbf{O}_{C,3V}) \\ 0 & \mathbf{0}_C^T & \mathbf{0}_C^T & \mathbf{0}_C^T & \mathbf{0}_C^T & t_{i-1}^x & 0 & 0 & (\mathbf{0}_V^T|\tau_{i-1}^x\mathbf{u_i}^T|\mathbf{0}_{2V}^T) \\ 0 & \mathbf{0}_C^T & \mathbf{0}_C^T & \mathbf{0}_C^T & \mathbf{0}_C^T & 0 & t_{i-1}^y & 0 & (\mathbf{0}_{2V}^T|\tau_{i-1}^y\mathbf{u_i}^T|\mathbf{0}_V^T) \\ 0 & \mathbf{0}_C^T & \mathbf{0}_C^T & \mathbf{0}_C^T & \mathbf{0}_C^T & 0 & 0 & e_{i-1} & (\mathbf{0}_{3V}^T|\gamma_{i-1}\mathbf{u_i}^T) \\ \mathbf{0}_P & \mathbf{O}_{P,C} & \mathbf{O}_{P,C} & \mathbf{O}_{P,C} & \mathbf{O}_{P,C} & \mathbf{0}_P & \mathbf{0}_P & \mathbf{0}_P & \mathbf{I}_P \end{pmatrix}, \tag{B1}$$

where C is the number of centers, $V = N_{\mathrm{views}} - 1$, $P = 4(N_{\mathrm{views}} - 1)$, $\mathbf{0}_n$ and $\mathbf{1}_n$ are column vectors containing all zeros and ones of length n, respectively, $\mathbf{O}_{m,n}$ is a zero matrix of size $m \times n$, $[\mathbf{q}] \equiv \mathrm{diag}(\mathbf{q})$ for an arbitrary vector $\mathbf{q}$, $\boldsymbol{\varepsilon} = \boldsymbol{\theta} + \gamma$, and $\mathbf{u_i}^T \equiv (\mathbf{0}_{i-2}^T\mathbf{1}\mathbf{0}_{V-(i-1)}^T)$ is a $1 \times V$ vector.

N. N. thanks Prof. P. K. Panigrahi (Dept. of Mechanical Engineering, IIT, Kanpur) for a very interesting discussion about physical experiments and situations with shape-reconstruction requirements. We thank the anonymous reviewer for pointing out directions of improvement in the presentation of our results.

References

1. A.-P. Tossavainen, M. Vauhkonen, and V. Kolehmainen, "A three-dimensional shape estimation approach for tracking of phase interfaces in sedimentation processes using electrical impedance tomography," Meas. Sci. Technol. **18**, 1413–1424 (2007).
2. V. Kolehmainen, S. Prince, S. R. Arridge, and J. P. Kaipio, "State estimation approach to the nonstationary optical tomography problem," J. Opt. Soc. Am. A **20**, 876–889 (2003).
3. S. Prince, V. Kolehmainen, J. P. Kaipio, M. A. Franceschini, D. Boas, and S. R. Arridge, "Time-series estimation of biological factors in optical diffusion tomography," Phys. Med. Biol. **48**, 1491–1504 (2003).
4. Y. Bresler and A. Macovski, "Three dimensional reconstruction from projections with incomplete and noisy

data by object estimation," IEEE Trans. Acoust. Speech Signal Process. **35**, 1139–1152 (1987).
5. K. J. Daun, S. L. Waslander, and B. B. Tulloch, "Infrared species tomography of a transient flow field using Kalman filtering," Appl. Opt. **50**, 891–900 (2011).
6. M. G. Twynstra, K. J. Daun, and S. L. Waslander, "Line-of-sight-attenuation chemical species tomography through the level set method," J. Quant. Spectrosc. Radiat. Transfer **143**, 25–34 (2014).
7. Y. Shi and W. C. Karl, "Dynamic tomography with curve evolution methods," in *Proceedings of 2002 IEEE International Conference on Acoustics, Speech, and Signal Processing*, Orlando, Florida, May 13–17, 2002 (IEEE, 2002), Vol. **4**, pp. 3229–3232.
8. Y. Shi, W. C. Karl, and D. A. Castanon, "Curve evolution methods for dynamic tomography with unknown dynamic models," Proc. SPIE **5032**, 675–683 (2003).
9. E. L. Miller, M. Kilmer, and C. Rappaport, "A new shape based object localization and characterization from scattered field data," IEEE Trans. Geosci. Remote Sens. **38**, 1682–1696 (2000).
10. A. D. Zacharopoulos, S. R. Arridge, O. Dorn, V. Kolehmainen, and J. Sikora, "Three-dimensional reconstruction of shape and piecewise constant region values for optical tomography using spherical harmonic parametrization and a boundary element method," Inverse Probl. **22**, 1509–1532 (2006).
11. S. R. Arridge, O. Dorn, J. P. Kaipio, V. Kolhemainen, M. Schweiger, T. Tarvainen, M. Vauhkonen, and A. D. Zacharopoulos, "Reconstruction of subdomain boundaries of piecewise constant coefficients of the radiative transfer equation from optical tomography data," Inverse Probl. **22**, 2175–2196 (2006).
12. R. Firoozabadi, E. L. Miller, C. M. Rappaport, and A. W. Morgenthaler, "Subsurface sensing of buried objects under a randomly rough surface using scattered electromagnetic field data," IEEE Trans. Geosci. Remote Sens. **45**, 104–117 (2007).
13. S. Babaeizadeh and D. H. Brooks, "Electrical impedance tomography for piecewise constant domains using boundary element shape-based inverse solutions," IEEE Trans. Image Process. **26**, 637–647 (2007).
14. N. Naik, J. Eriksson, P. de Groen, and H. Sahli, "A nonlinear iterative reconstruction and analysis approach to shape-based approximate electromagnetic tomography," IEEE Trans. Geosci. Remote Sens. **46**, 1558–1574 (2008).
15. E. T. Chung, T. F. Chan, and X. C. Tai, "Electrical impedance tomography using level set representation and total variation regularization," J. Comput. Phys. **205**, 357–372 (2005).
16. O. Dorn and D. Lesselier, "Level set methods for inverse scattering," Inverse Probl. **22**, R67–R131 (2006).
17. N. Naik, R. Beatson, J. Eriksson, and E. van Houten, "An implicit radial basis function based reconstruction approach to electromagnetic shape-tomography," Inverse Probl. **25**, 025004 (2009).
18. A. Aghasi, I. Mendoza-Sanchez, E. L. Miller, C. A. Ramsburg, and L. M. Abriola, "A geometric approach to joint inversion with applications to contaminant source zone characterization," Inverse Probl. **29**, 115014 (2013).
19. A. Aghasi, M. Kilmer, and E. Miller, "Parametric level set methods for inverse problems," SIAM J. Imaging Sci. **4**, 618–650 (2011).
20. A. Blake and M. Isard, *Active Contours* (Springer-Verlag, 1998).
21. N. Morrison, *Tracking Filter Engineering: The Gauss-Newton and Polynomial Filters* (IET, 2012).
22. F. Santosa, "A level set approach for inverse problems involving obstacles," ESAIM Control Optim. Calc. Var. **1**, 17–33 (1996).
23. T. F. Chan and L. Vese, "Active contours without edges," IEEE Trans. Image Process. **10**, 266–277 (2001).
24. N. Naik, R. M. Vasu, and M. R. Ananthasayanam, "Single-resolution and multiresolution extended-Kalman-filter-based reconstruction approaches to optical refraction tomography," Appl. Opt. **49**, 986–1000 (2010).
25. R. Kress, *Linear Integral Equations* (Springer-Verlag, 1999).
26. A. Presley, *Elementary Differential Geometry* (Springer-Verlag, 2001).
27. A. H. Andersen and A. C. Kak, "Digital ray tracing in two dimensional refractive fields," J. Acoust. Soc. Am. **72**, 1593–1606 (1982).
28. J. Nocedal and J. Wright, *Numerical Optimization*, Springer Series in Operations Research (Springer, 1999).